Interfacial Phenomena in Polymer Films and Generation of Maxwell Displacement Current

Mitsumasa Iwamoto

Department of Physical Electronics, Tokyo Institute of Technology,
2-12-1 O-okayama, Meguro-ku, Tokyo 152-8552, Japan
E-mail: iwamoto@pe.titech.ac.jp

Summary: Interfacial electrostatic phenomena in ultrathin polyimide films have been examined, and the space charge distribution and electronic density of states have been determined. The presence of excess negative charges at the film-metal interface of nanometer thickness has been revealed and the alignment of the surface Fermi level of polymer films and Fermi level of metals have been elucidated. Taking into account the interfacial space charge, a step structure observed in the I-V characteristic of metal-polyimide-rhodamine-polyimide-metal junction, very similar to Coulomb staircase, is well explained. Furthermore, the electrical breakdown mechanism of a nanometer-thick polyimide film is found quite different from that of micrometer-thick films, owing to the presence of this interfacial nanometric space charge. Finally, for a profound understanding of the behaviour of surface monolayer, the Maxwell displacement current measurement coupled with optical second harmonic generation measurement has been employed.

Keywords: Maxwell-displacement current; polyimide; SHG; single electron tunnelling; surface potential

Introduction

Many organic materials that are interesting in electronics have been synthesized and discovered during last several decades.[1,2] We can see one of the most remarkable achievements of Heeger, MacDiarmid and Shirakawa awarded by the Nobel Prize in Chemistry 2000, due to their contribution to the discovery and development of conductive polymers.[3-5] In the hope of observing novel and useful electric and optical properties, many investigations have been carried out to build organic devices, taking into account specific physical properties of organic films such as flexibility, lightness and others. Plastic solar cells, flexible-type field-effect transistors (FETs), electroluminescent (EL) devices and others have been developed along with the development of new organic materials.[6] Insightful ideas have also been proposed to open new methods and device technologies in molecular electronics.[7] However, these are no longer sufficient. Profound understanding of nanointerfacial phenomena is essential. It is needless to say

 DOI: 10.1002/masy.200450804

that one of the most primitive but important applications of organic thin films is to use them as tunneling barriers. Thus there has been a growing interest in the preparation of high-quality organic ultrathin films during the last several decades. As a result, the preparation technique has greatly advanced, and many important organic films have been successfully prepared.[8] Among them are polyimide (PI) and polyethylene Langmuir-Blodgett (LB) films, which function as tunneling spaces.[9] Briefly, for example, the monolayer thickness of the prepared PI LB film is 0.4 nm. The PI LB films are almost pinhole-free, and they are thermally and chemically stable up to a temperature of 400 ℃. They exhibit excellent electric-insulating properties, and function as tunneling barriers in tunnel junctions such as Josephson junctions. The success of the preparation of excellent insulating ultrathin films and other semiconductor films motivated the authors to study the interfacial electronic phenomena in electric-insulating films, semiconductor films, etc,[10] because the *I-V* characteristic of thin films is controlled by electrostatic interfacial phenomena. The surface potential method, Maxwell displacement current measurement and optical second harmonic generation (SHG) measurement have been employed in elucidating nanometric interfacial phenomena. In this paper, the study of polymer films to clarify the interfacial phenomena has been reviewed. Then a step structure, similar to Coulomb staircase, observed in current-voltage (*I-V*) characteristics of junctions using rhodamine-dendrimer molecules [11,12] is discussed in association with the interfacial nanometric phenomena.[13,14] Furthermore, the electrical breakdown process of ultrathin film is discussed in association with the space charge phenomena. Finally, Maxwell displacement current measurement coupled with optical second harmonic generation measurement used to clarify the surface molecular motion is briefly introduced.

Interfacial Electrostatic Phenomena in Ultrathin Films

For a better understanding of the interfacial electrostatic phenomena, it is helpful to use ultrathin films whose thickness is less than the electrostatic double layer formed at the film/metal interface, and then to gain information on the distribution of the electronic density of states as well as on the space charge distribution of excess charges in the films prepared on metal electrodes. LB films are suitable because they can be prepared on solid substrates by the layer-by-layer deposition with monolayer thickness. In combination with the LB deposition technique and the surface potential method, one can examine space charge distribution as well as the density of

states in ultrathin films.[13,14] PI LB films deposited on Au, Cr, and Al base electrodes were examined after the heat treatment for more than one hour at a temperature of 150 ℃ in vacuum. The surface potential of PI LB films was measured with reference to the potential of the clean base metal electrodes. The surface potentials gradually decreased as the number of deposited layers increased, and then reached a constant saturated potential at the number of 20-50 layers. These results indicated that PI LB films acquired electrons from metal, and an electrostatic layer was thus formed at the metal/PI LB film interface within a region of nanometer thickness. Interestingly, the surface potential value in PI LB films shifted negatively as the temperature increased, indicating that the tendency of PI to accept electrons becomes stronger as the temperature increases. The surface potential V_S built across PI LB films on metal is given by

$$V_S = \int_0^D \frac{x\rho(x)}{\varepsilon_0\varepsilon_r} \mathrm{d}x = \frac{\bar{x}Q}{\varepsilon_0\varepsilon_r}, \quad (1)$$

$$\text{with } \bar{x} = \frac{\int_0^D x\rho(x)\,\mathrm{d}x}{Q} \text{ and } Q = \int_0^D \rho(x)\,\mathrm{d}x.$$

Here, ε_0 is dielectric permittivity of vacuum, ε_r (= 3.2) is the relative permittivity of PI, D is the film thickness, x is the distance from the metal electrode, $\rho(x)$ is the space charge density at location x, $\bar{x}$ is the mean location of the excess charges displaced from the electrodes, and Q is the total charge displaced from the metal electrodes. Differentiation of surface potential V_S with respect to the film thickness D gives a quantity proportional to the space distribution of charges $\rho(D)$. Using the surface potential measurement, the relationship between V_S and the number of deposited layers n, proportional to the film thickness D, is calculated. Thus $\rho(D)$ can be estimated. Figure 1 shows an example of the space charge density $\rho(D)$ in PI LB film at a temperature of 25 ℃. The space charge density decreases steeply as the number of layers increases. Most of the excess charges exist in PI LB films within the distance of 4 nm from electrodes. Ca. 1 - 10 % of monomer units of PI accept electrons from metal electrodes in this region, in which the density of PI molecule unit is about 3×10^{27} m^{-3}. A linear relationship with a slope of unity was observed between the work function of metals and the saturated surface potential of PI. This relationship indicates that a thermodynamic equilibrium was established at the PI LB film/metal interface. In other words, electronic charges are transferred at the interface

between PI films and metals until the surface Fermi level of PI and the Fermi level of metal electrodes are in coincidence.[14] Similar results were obtained for other LB films.[15] As described above, we may have the prediction that excess electronic charges exist at the film-metal interface.

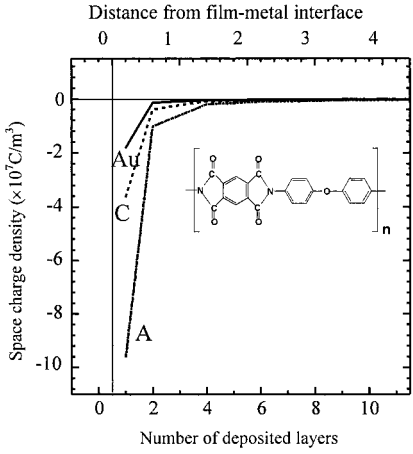

Figure 1. Interfacial space charge distribution in polyimide LB film at film-metal interface at room temperature.

MIM junction with rhodamine molecule

As mentioned in the previous section, excessive electronic charges transferred from metals to PI LB films exist at the metal/PI interface of an LB film . This interfacial space charge forms a very high-electric field of the order of $10^8 - 10^9$ V/m at the interface and directly affects the electron transport through PI LB films as well as the electrical breakdown in the films. The Schottky-type behavior in the current-voltage (*I-V*) and capacitance-voltage (*C-V*) characteristics of polyimide LB films can be successfully explained by taking into account the space charge field.[16] Similar discussion with consideration of interfacial space charge is also valid to explain the I-V characteristic of electron tunneling junctions in a structure of Au/ PI/ rhodamine dendrimer / PI/ Al, where a step *I-V* structure, very similar to Coulomb staircase behavior, is observed.[12,13] In more detail, the junctions with structures Au/PI (25)/PI:Rh-G2 (molar ratio 1:1, and 500:1)/PI (30)/Al junctions (junction area 0.25 mm^2) were prepared using Au and Al electrodes. Rh-G2 is

rhodamine dendrimer whose chemical structure is shown in Fig. 2. The number in the parenthesis represents the number of deposited layers. It was supposed that the prepared Au/PI (25)/PI:Rh-G2 (1)/PI (30)/ Al junction (electrode area : 0.25 mm^2) consisted of about 5.4×10^8 small elements with the same structure. Here the number of small elements was calculated using the limiting molecular area estimated from the surface pressure area isotherm of Rh-G2 monolayer.

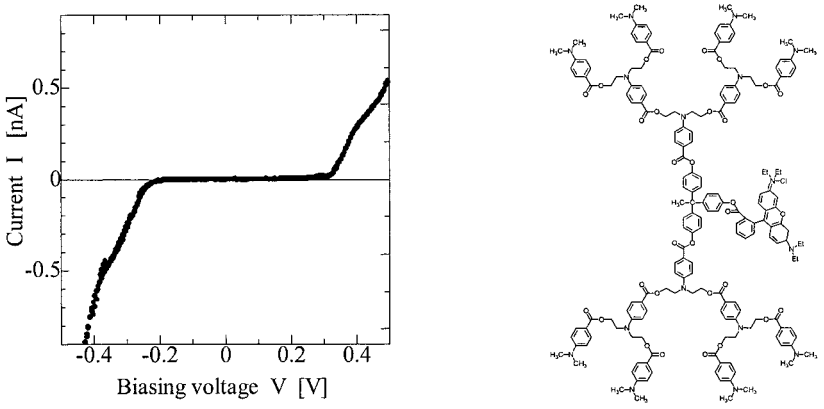

Figure 2. The *I-V* characteristics of Au/PI (25)/PI:Rh-G2 (1)/PI (30)/Al junction. The rhodamine dendrimer (Rh-G2) structure is given.

Figure 2 shows a typical *I-V* characteristic of the junction at a temperature of 30 K, where a dc step voltage was applied to the top Al electrode with reference to the base Au electrode with a step of 0.003-0.005 V. In the figure, the step structure is clearly observed; the *I-V* steps can be seen at voltages of 0.3 V and -0.25 V. Similar experimental results were obtained for junctions with on top Au electrode. On the other hand, no step structure was seen in junctions without rhodamines. These results suggest that Rh-G2 molecules make a main contribution to the creation of step structure. The *I-V* characteristic is controlled by the single-electron tunneling via rhodamine molecule. However, to explain the behavior of the *I-V* step structure, it is necessary to take into account the interfacial space charge and residual charge. In what follows, we show the analysis, where the rhodamine molecule is assumed to function as a quantum dot (central electrode).

According to the theory of Coulomb blockade,[17] the *I-V* step structure appears at a voltage of

$$V = \frac{1}{C_f}(n + \frac{1}{2})e \quad (n = 0, \pm 1, \pm 2, \pm 3, \ldots), \tag{2}$$

if the contribution of space charge, i.e., the so-called "back ground charge", and residual charge are discarded. Here C_f is the capacitance formed between the quantum dot and metal electrodes, and e is electron charge. Using the image charge method in the electromagnetic field theory (see Fig. 3a, the capacitance C_0 formed between a sphere metal (quantum dot) and plane metal electrode is calculated as[11,18]:

$$C_0 = 4\pi\,\varepsilon_0\, r\, F(y) \qquad \text{with} \quad F(y) = \sum_{i=0}^{\infty} \frac{\sinh y}{\sinh(i+1)\,y} \tag{3}$$

assuming r is the radius of the sphere metal; y is given by $y = \ln(s + \sqrt{s^2 - 1})$ with $s = z_h/r+1$. z_h is the distance between the sphere and plane electrode (see Fig. 3a). It is instructive to note that the capacitance of the sphere with radius r in a free space is given by $4\pi\varepsilon_0 r$. Therefore, in Eq.(3), it expresses the effect of the sphere approaching the plane electrode. C_0 is nothing but the geometrical capacitance and it is replaced by $C_M = \varepsilon\, C_0$ when the sphere-plane electrode system is placed in a medium with permittivity ε .

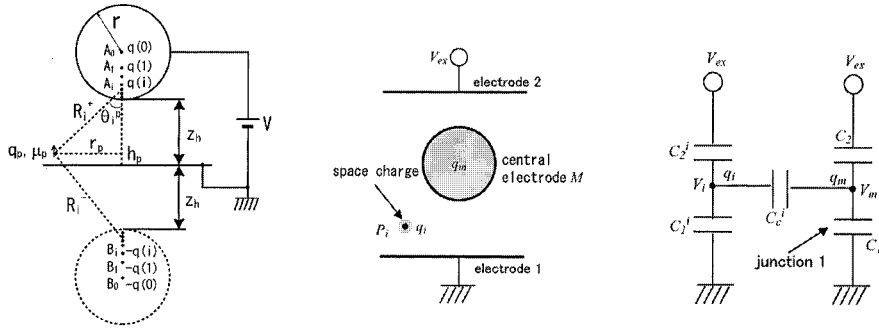

Figure 3. (a) Image charges and sphere-plane electrode system. (b) Model structure of our junction. (c) Equivalent circuit.

Figure 3b shows the model structure of our junction, where central electrode M is sandwiched between two electrodes separated by tunneling barriers.[19] In this case, the tunneling barrier is PI LB film. The central electrode M is a spherical electrode with a radius r, and this is the

rhodamine molecule (Rh-G2). This modeling is very simple, but does not lose the underlying physics for the understanding of the *I-V* step structure shown in Fig. 2. Between the central electrode M and outer two electrodes 1 and 2, capacitance C_1 and C_2 are formed. C_1 and C_2 are the capacitance C_M mentioned above, and the capacitance C_f is given by $C_1 + C_2$. Thus the *I-V* step structure appears at a voltage given by Eq. (2) when the contribution of space charge and residual charge is minor. However, this is not true when the interfacial space charge is present as shown in Fig. 1.

First, in order to clarify the space charge behavior, charge q_i is assumed to site in position P_i. This charge couples to the central electrode and outer two electrodes with coupling capacitance C_C^i, C_1^i and C_2^i, respectively, and then the equivalent circuit model is obtained as shown in Fig. 3c. Charge q_M is induced on central M due to the presence of charge q_i. Using this equivalent circuit and then to calculate the energy ΔW due to the increase in charge q_m from $-ne$ to $-ne+1e$ (n is the number of electrons) by electron tunneling across the capacitance C_1, we obtain the external voltage V_{ex} for the electron tunneling as[18,19]:

$$V_{ex} \geq \frac{1}{C_2 g_2}\left\{\left(n+\frac{1}{2}\right)e-\frac{C_c^i}{C_\Sigma^i}q_i\right\} \tag{4}$$

with $g_2 = 1+\frac{C_c^i}{C_\Sigma^i}\cdot\frac{C_2^i}{C_2}$ and $C_\Sigma^i = C_1^i + C_2^i + C_2^i$. Here g_2 represents the effect of coupling capacitance and $q_i C_c^i / C_\Sigma^i$ represents the space charge effect. However, if we take into account the difference in the work function between central metal electrode and two outer electrodes, Eq. (4) is replaced by

$$V_{ex} \geq \frac{1}{C_2 g_2}\left\{\left(n'+\frac{1}{2}\right)e-V_D C_f-\frac{C_c^i}{C_\Sigma^i}q_i\right\},\ (n'=\cdots-2,-1,0,1,2,\cdots), \tag{5}$$

with $n' = n + k$, $C = C_1 + C_2$ and $f = 1 + f_i$ with $\frac{C_c^i}{C_\Sigma^i}\left(\frac{C_1^i + C_2^i}{C_1 + C_2}\right)$. Here k is an integer chosen to satisfy the relation $\left|V_D C_f + \frac{C_c^i}{C_\Sigma^i}q_i - ke\right| \leq \frac{e}{2}$. The reason is that the accurate alignment in the Fermi

levels of central electrode and outer electrodes never happens, and the displacement of one electron from outer electrodes into central electrode builds up the additional potential $e/(C_1+C_2)$. V_D in Eq.(5) is the residual voltage and expresses the difference in the Fermi energies between the central metal electrode and outer electrodes under a short circuit condition. Furthermore, ke represents the charge that should be redistributed due to the additional potential established in the short circuit condition. The induced charge $q_i C_c^i / C_\Sigma^i$ on electrode M can be calculated if the potential V_i in position P_i in Laplace field is known. Similarly, in the presence of excessive charges q_i (i = 1, 2, 3, ...) surrounding the central metal M, the following relation (6) is obtained in replacing Eq.(5). That is

$$V_{ex} \geq \frac{1}{C_2 G_2}\left\{\left(j+\frac{1}{2}\right)e - V_D CF - \Delta Q\right\}, \quad (j = \cdots -2, -1, 0, 1, 2, \cdots). \tag{6}$$

Here $F = 1 + \sum_i f_i$, $G_2 = 1 + \sum_i (C_c^i / C_\Sigma^i)\cdot(C_2^i / C_2)$, and $\Delta Q = \sum_i (C_c^i / C_\Sigma^i) q_i$.

From Eq.(6) we find that the space charge field and residual charge make a significant contribution to the *I-V* characteristic.

On the basis of the above analysis, the *I-V* step structure shown in Fig. 2 can be argued as follows: The induced charge ΔQ is approximately given by

$$\Delta Q = C_1 G_1 V_{s1} - C_2 G_2 V_{s2} \quad \text{with} \quad G_1 = 1 + \sum_i (C_c^i / C_\Sigma^i)\cdot(C_1^i / C_1). \tag{7}$$

Here V_{s1} and V_{s2} are surface potentials built at the film-metal interface, given by Eq. (1). The surface potentials of about -200 mV and -1000 mV are built at PI/Au and Al/PI interface at room temperature. If the space charge density is high at the interface, the relation $C_1 G_1 = C_2 G_2$ is approximately satisfied. Using Eq. (7), the shift of step voltage $|\Delta V|$ is estimated to be less than 1200 mV. However, this shift must satisfy the relation given by $|\Delta V| \leq e/2C_2G_2 \,(= e/2C_1G_1)$ (see Eqs. (5) and (6)). For our junctions of Au/PI/Rh-G2/PI/Al, the capacitance formed between Rh-G2 and metal electrode is estimated to be of the order of 10^{-19} F. Thus, $|\Delta V| \leq 800$ mV is expected. This speculation well supports our experimental result shown in Fig. 2. Figure 4 shows the theoretical and experimental d*I*/d*V*-*V* characteristics of Au /PI /Rh-G2 /PI /Al junction at a temperature of 33 K. The theoretical line was calculated in a manner similar to that in the analysis

of *I-V* characteristics of double barrier tunneling junction.[20] For $C_2 = 2.39 \times 10^{-19}$ F, $C_1 = 2.76 \times 10^{-19}$ F and $Q\text{-}Q_0 + ke = 8.37 \times 10^{-21}$ C, the calculated line shows an agreement with the experimental plots. As mentioned above, the *I-V* step structure is explained by taking into account the presence of space charge and residual charge.

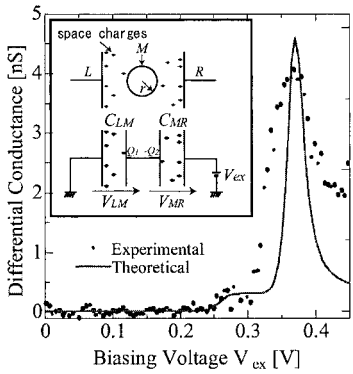

Figure 4. The theoretical and experimental d*I*/d*V*-*V* characteristic of Au-/PI/Rh-G2/PI/Al junction.

The *I-V* measurement was carried out under the scanning tunneling microscope (STM) operation and the step-structure was obtained. Furthermore, we recently succeeded in the detection of a similar *I-V* step structure using metal PI-metal junctions with including C60 molecules prepared by the spin-coating technique.

Electric breakdown of ultrathin films

The study of electrostatic interfacial phenomena at organic film/metal interfaces is obviously important in electronics and electrical insulation, and they have been a continuous research subject since the discovery of contact electrification.[21,22] As mentioned earlier, the nanometric interfacial electrostatic charges make a significant contribution to electric conduction. Similarly, the electrical breakdown will be controlled by the formation of space charge, though to show this is not an easy task, owing to the difficulty in preparation of sophisticated organic ultrathin films. The information on interfacial space charge distribution obtained by the surface potential study will help in elucidating the electrical breakdown process. To examine the electrical breakdown

mechanism, we measured the surface potential of PI LB films on Al, Ag and Au electrodes, which were charged by a dc voltage in a needle plane electrode system. We then studied the electrical breakdown process in ultrathin PI LB films in association with the interfacial electrostatic phenomena.[23] Briefly, a needle electrode (point angle 30° and curvature radius 10 μ m) was placed above the sample in a vacuum vessel, at a distance d of 1 mm from the sample. The samples were charged by applying a dc voltage between –2.5 kV and +2.5 kV to the needle electrode for 20 min, and then the surface potential of the charged samples was examined. Whilst the samples were charged, some of them were electrically broken. When 50 % of the samples were electrically broken by the application of biasing voltage, we defined this voltage as the breakdown voltage. The surface potential of charged samples decreased as the dc biasing voltage increased, as shown in Fig. 5. Usually, electrically insulating polymer films are charged with electronic homo-charges when the polymers are non-polar and do not possess extrinsic ionic impurities. That is, the surfaces of films are negatively charged by the application of negative voltages to the needle electrode with respect to the plane electrode, whereas these are positively charged by the application of positive voltages. However, the experimental results for PI LB films were opposite to this prediction. Furthermore, the breakdown voltage increases as the work function of metals increases (work-function, Au > Cu > Al), and it depends on the polarity of biasing voltages. As mentioned earlier, the surface potential V_s is built across the PI LB films. At equilibrium, the surface Fermi level of PI LB films and the Fermi level of metals are brought into coincidence at the interface: the electronic states of PI, whose electronic energy is higher than the Fermi level of the metal, can donate electrons to the metal if the states are filled with electrons before electrification. By contrast, the electronic states of PI whose electronic energy is lower than the Fermi level of the metal, can accept electrons from the metal if the states are vacant. On the basis of this model, we may argue the result shown in Fig. 5 as follows. PI LB films are negatively charged even when biasing voltage is zero (see Fig. 1). The PI LB films are more negatively charged by applying a positive biasing voltage to the needle electrode, whereas they are gradually positively charged as the biasing voltage becomes more negative. A possible explanation is that the mean location of electronic charges $\bar{x}$ and the total charge Q given by Eq. (1) increase by application of positive biasing voltage, whereas they decrease by the application of negative biasing voltage. Thus we may expect that electrons are injected from base electrodes

to PI LB films via interfacial states at the film/metal interface when the needle electrode is positively biased, whereas holes are injected into PI LB films when the needle is negatively biased. In other words, the main contribution of excessive charge is electrons injected from metal electrodes, and not electron charges deposited on film surface from the side of needle electrode. The experimental result shown in Fig. 5 can be explained in this way. Similarly, the dependence on the number of deposited layers, the nature of metal electrode and others can be explained in the same way.

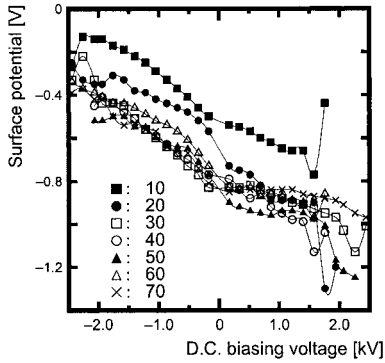

Figure 5. Relationships between the surface potentials and the number of deposited layers for PI LB films on Al electrodes. The abrupt change of the surface potential around dc biasing voltage of +1.5 and –2.0 kV is due to the breakdown.

MDC and SHG study of surface monolayers

As mentioned earlier, the electrical transport property of monolayers is strongly dependent on the nanometric dielectric phenomena observed at the interface. In this sense, it is also very important to clarify the behavior of polar molecules at the interface in association with the dielectric phenomena, though the dipolar polarization was not so important for PI LB films. Generally, the orientational distribution of polar molecules gives rise to the spontaneous polarization at the interface, and Maxwell displacement current and SHG are generated from non-centrosymmetric structured monolayers[10,24] Monolayers of liquid crystals, polymers and other materials have been examined using this technique. For example, the azobenzene dendrimer monolayer on water surface has been examined using the MDC measurement, and the dipole moment was determined in association with the molecular motion of constituent molecules. The calculated dipole moment

was in good agreement with the calculation based on the semiempirical molecular orbital (MO) calculation.[25] Further, MDC and SHG measurements have been employed for liquid crystal monolayers, and the orientational order parameters of constituent LC molecules have been determined.[26] This information will be important to clarify the electrical transport in ultrathin films as well as for the control of electron motion such as light-driven molecular current, [27] and others.

Conclusion

The surface potential of PI LB films in a needle plane electrode system was examined. It was concluded that the main contribution to the creation of the surface potential was electron excess charges injected from the metal electrodes via interfacial states in PI LB films at the film/metal interface. Furthermore, the interfacial space charge also makes a significant contribution to the I-V characteristic of organic junctions and the electrical breakdown of ultrathin films.

[1] *Special issue on Functional Organic Materials for Devices*, J. Mater. Chem. **1999**, 9, 1853.
[2] *Organic Thin Films*, Materials Chemistry Discussion No. 2, J. Mater. Chem. **2000**, 10, 1.
[3] A. J. Heeger, Rev. Mod. Phys. **2001,** 73, 681 (Nobel Lectures).
[4] A. G. MacDiamid, Rev. Mod. Phys. **2001,** 73, 701 (Nobel Lectures).
[5] H. Shirakawa, Rev. Mod. Phys. **2001,** 73, 713 (Nobel Lectures).
[6] C. J. Brabec, N. S. Sariciftci and J. C. Hummelen, Adv. Funct. Mater. **2001,** 11, 15.
[7] C. Joachim, J. K. Gimzewski and A. Aviram, Nature **2000**, 408, 541.
[8] H. S. Nalwa, *Supramolecular Photosensitive and Electractive Materials*, Academic Press, San Diego 2001.
[9] M. Iwamoto and M. Kakimoto, in: *Polyimides, Fundamentals and Application,* M.K. Ghosh and K.L. Mittal, Eds., Marcel Dekker, Inc., New York, 1996, p. 815/884ff.
[10] M. Iwamoto and C. X. Wu, *The Physical Properties of Organic Monolayers*, World Scientific, Singapore 2001.
[11] Y. Noguchi, Y. Majima and M. Iwamoto, J. Appl. Phys. **2001,** 90, 1368.
[12] Y. Noguchi, M. Iwamoto, T. Kubota and S. Mashiko, J. Appl. Phys. **2002,** 94, in press.
[13] M. Iwamoto, A. Fukuda and E. Itoh, J. Appl. Phys. **1994, 75,** 1607.
[14] E. Itoh and M. Iwamoto, J. Appl. Phys. **1997**, 81 1790.
[15] M. Iwamoto, J. Mater. Chem. **2000**, 10, 99.
[16] C. Q. Li, Y. Noguchi, H. C. Wu and M. Iwamoto, Jpn. J. Appl. Phys. **2001,** 40, 4575.
[17] S. Carraral, in *Nanoparticles and Nanostructured Films,* F.H. Fendl, Ed., Wiley-VCH, Weinheim, 1998, Chap.15.
[18] M. Iwamoto, Y. Noguchi, T. Kubota and S. Mashiko, Curr. Appl . Phys. **2002**, in press.
[19] Y . Noguchi, M. Iwamoto, T. Kubota and M. Mashiko, Jpn. J. Appl. Phys. **2002**, 41, 2749.
[20] A . E. Hanna and M .Tinkham, Phys. Rev. B **1991**, 44, 5919.
[21] J. Lowell and A. C. Rose-Innes, Adv. Phys. **1980**, 29 947, and references therein.
[22] L. H. Lee, J. Electrostatics **1994**, 32, 1, and references therein.
[23] M. Fukuzawa and M. Iwamoto, IEEE Trans. Dielec. Electri. Insul. **2001**, 8, 832.
[24] Y. R. Shen, *The Principles of Nonlinear Optics*, Wiley, New York, 1984.
[25] T. Manaka, D. Shimura and M. Iwamoto, Chem. Phys. Lett. **2002**,355, 164.
[26] A. Tojima, T. Manaka and M. Iwamoto, J. Chem. Phys. **2001**, 115, 9010.
[27] S. Nespurek and J. Sworakowski, Thin Solid Films **2001**, 393, 168.